Journal of Ocean Engineering and Marine Energy

The MBARI-WEC: a power source for ocean sensing

--Manuscript Draft--

Manuscript Number:	
Full Title:	The MBARI-WEC: a power source for ocean sensing
Article Type:	Research Article
Funding Information:	Office of Energy Efficiency and Renewable Energy — Not applicable
Abstract:	Interest in wave energy converters to provide autonomous power to various ocean-bound systems, such as autonomous underwater vehicles, sensor systems, and even aquaculture farms, has grown in recent years. The Monterey Bay Aquarium Research Institute has developed and deployed a small two-body point absorber wave energy device suitable to such needs. This paper provides a description of the system. Additionally, to support future control design and system modification efforts, a set of hydrodynamic models are presented and cross-compared. To test the viability of using a linear frequency-domain admittance model for controller tuning, the linear model is compared against four WEC-Sim models of increasing complexity. The linear frequency-domain model is found to be generally adequate for capturing system dynamics, as the model agreement is good and the degree of nonlinearity introduced in the WEC-Sim models is generally less than 2.5%.
Corresponding Author:	Ryan G. Coe, PhD Sandia National Laboratories UNITED STATES
Corresponding Author Secondary Information:	
Corresponding Author's Institution:	Sandia National Laboratories
Corresponding Author's Secondary Institution:	
First Author:	Andrew Hamilton, PhD
First Author Secondary Information:	
Order of Authors:	Andrew Hamilton, PhD
	François Cazenave
	Dominic Forbush, PhD
	Ryan G. Coe, PhD
	Giorgio Bacelli, PhD
Order of Authors Secondary Information:	
Author Comments:	
Suggested Reviewers:	George Hagerman, MS ODU hagerman@ccpo.odu.edu Expertise in wave energy and blue economy applications
	Rob Cavagnaro PNNL robert.cavagnaro@pnnl.gov Expertise in blue economy applications for marine renewables.
	Nathan Tom NREL Nathan.Tom@nrel.gov Expertise in WEC-Sim, WEC modeling, and WEC control.

Keywords:	Wave energy converter (WEC); blue economy; hydrodynamic modeling

Journal of Ocean Engineering and Marine Energy manuscript No.
(will be inserted by the editor)

The MBARI-WEC: a power source for ocean sensing

Andrew Hamilton · François Cazenave · Dominic Forbush · Ryan G. Coe · Giorgio Bacelli

Received: date / Accepted: date

Abstract Interest in wave energy converters to provide autonomous power to various ocean-bound systems, such as autonomous underwater vehicles, sensor systems, and even aquaculture farms, has grown in recent years. The Monterey Bay Aquarium Research Institute has developed and deployed a small two-body point absorber wave energy device suitable to such needs. This paper provides a description of the system. Additionally, to support future control design and system modification efforts, a set of hydrodynamic models are presented and cross-compared. To test the viability of using a linear frequency-domain admittance model for controller tuning, the linear model is compared against four WEC-Sim models of increasing complexity. The linear frequency-domain model is found to be generally adequate for capturing system dynamics, as the model agreement is good and the degree of nonlinearity introduced in the WEC-Sim models is generally less than 2.5%.

Keywords Wave energy converter (WEC) · blue economy · hydrodynamic modeling

A. Hamilton · F. Cazenave
Monterey Bay Aquarium Research Institute, CA, USA
Tel.: +1-831-775-1861
Fax: +1-831-775-1646
E-mail: [hamilton,francois]@mbari.org

D. Forbush · R.G. Coe · G. Bacelli
Sandia National Labs, Albuquerque, NM, USA
Tel.: +1-505-845-9064
Fax: +1-505-844-6541
E-mail: [dforbus,rcoe,gbacell]@sandia.gov

1 Introduction

While much of the work to date on WECs has been targeted at “utility-scale” devices, which would have capacities on the order of 1 MW, in line with wind turbines, there is now increasing interest in smaller devices. Smaller WECs may be used for a more distributed approach (i.e., with a “farm” of many WECs needed to give a MW of generating capacity as suggested by Falnes and Hals 2012) or for applications where the power needs are lower, such as the so-called blue economy (LiVecchi et al. 2019). Such a device might be used to power remotely located sensors or charge autonomous vehicles (Green et al. 2019; Driscol et al. 2020; Hagerman 2002).

This paper provides an overview of the Monterey Bay Aquarium Research Institute (MBARI) wave energy converter (WEC) – the device is herein referred to as the “MBARI-WEC.” The MBARI-WEC was originally developed in 2009 in order to provide power to MBARI’s various research missions. The project was initially funded by the Defense Advanced Research Projects Agency (DARPA), as a three-month grant to assess the availability of wave power around the world, and to assess DARPA’s previous attempts to generating electrical power from ocean waves. The project has been continued since then, with support from MBARI’s main funding source, the David and Lucille Packard Foundation.

First, a detailed description of the system is provided (Section 2). Next, in order to support future control design and system re-design efforts, a series of hydrodynamical models are proposed and cross-compared (Sections 3-4). These findings are discussed and summarized in Sections 5 and 6, respectively.

2 Device description

The MBARI wave-energy conversion buoy is a two-body point absorber that consists of a surface buoy and submerged heave-plate connected by an electro-hydraulic power take-off unit. A layout diagram is shown in Fig. 1 and key parameters for the device are given in Table 1. Power and communications extend from the buoy down to the heave-cone, but do not extend to the sea floor at this time. Typically, the system is deployed with the submerged heave cone anchored to the sea floor with a chain-catenary mooring and a 180 kg (400 lb) "Dormor" anchor. The usual deployment location is 36.7436 N, -121.88 E in roughly 80 m of water (Fig. 2).

The computing and software architecture of the system is distributed, as shown in Fig. 3, using micro-controllers in critical roles and a topside Linux computer to log telemetry, issue commands to the micro-controllers when needed, and provide shore-based control of the system. In particular, there are four micro-controllers throughout the system, serving as a battery controller (BC), a power-converter controller (PC), a pneumatic-spring controller (SC), and a heave-cone trefoil controller (TC). The locations of each of these micro-controllers is shown in Fig. 1. A listing of telemetry signals provided by each micro-controller is presented in Table 6 in the Appendix.

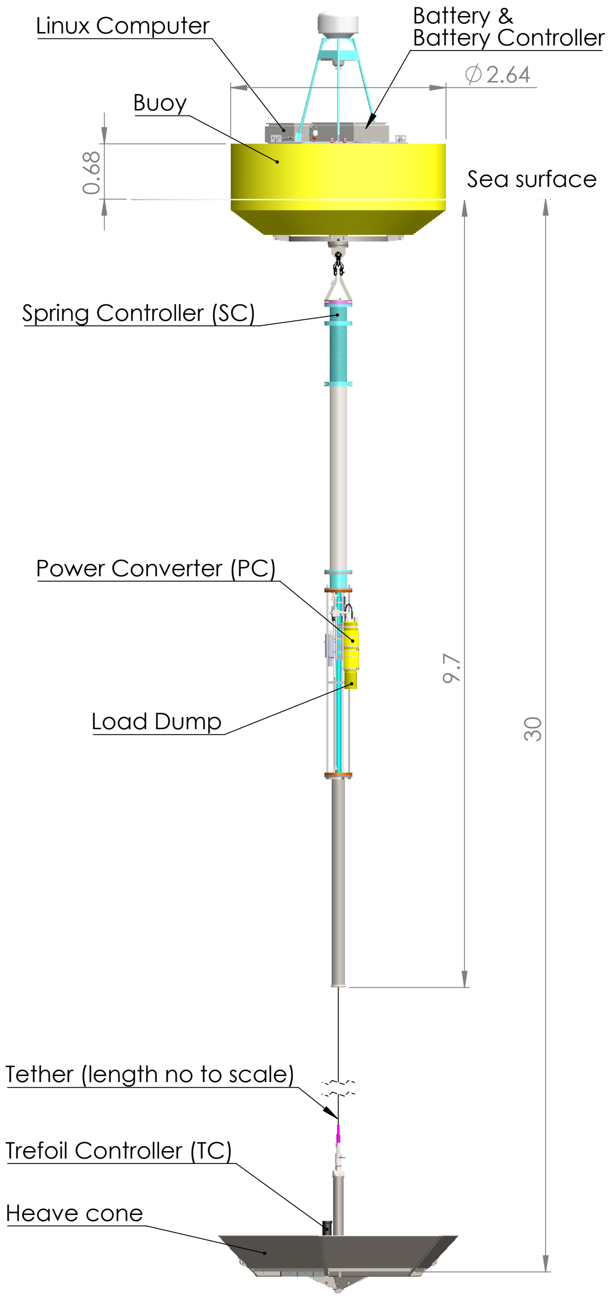

Fig. 1 MBARI-WEC system diagram showing mechanical layout along with electronic subsystem locations.

In each case, these controllers broadcast a stream of data on a Controller Area Network (CAN) bus continuously at 10-50 Hz. This data streams at 10Hz by default but the rate can be increased to up to 50 Hz when needed for control purposes. The topside Linux computer time-stamps and logs all of this data, and provides a mechanism for data transmission to shore via terrestrial radio or cell-phone modem. Each micro-controller can also accept commands from the Linux computer to execute a function or change behavior. In all cases, these controllers are fail-safe, if the Linux computer fails or communications is lost, each controller defaults to a rational behavior. This distributed computing infrastructure with the critical roles relegated to the

Table 1 MBARI-WEC key parameters.

Parameter	Value	Notes
Total system mass, m_t [kg]	2530	includes PTO system
PTO pneumatic spring const., K_{spring} [kN/m]	8.9	spring not purely linear, see Section 2.3
Buoy		
Mass, m_1 [kg]	1080	
Natural period, $T_{1,0}$ [s]	1.4	see Fig. 8
Center of mass, $z_{1,cog}$ [m]	0.67	below buoy deck, see ‘G’ mark in Fig. 4
Center of buoyancy, $z_{1,cob}$ [m]	0.98	below buoy deck, see ‘B’ mark in Fig. 4
Metacentric height [m]	1.93	
Water line [m]	0.80	below buoy deck (when PTO and heave cone are attached)
Water plane area, A_{wp} [m^2]	5.47	
2^{nd}-moment of area of water plane [m^4]	1.37	
Heave cone		
Mass, m_2 [kg]	815	
Natural period, $T_{2,0}$ [s]	7.9	see Fig. 8
Center of mass, $z_{2,cog}$ [m]	1.25	below attachment point, see ‘G’ mark in Fig. 5
Depth location [m]	30	see Fig. 1

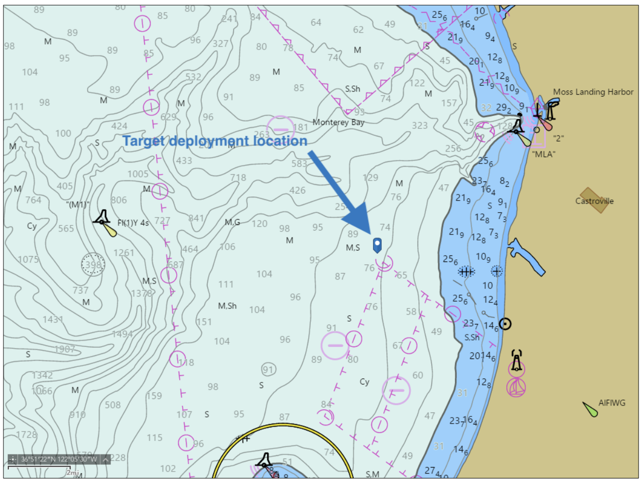

Fig. 2 Monterey Bay bathymetry at deployment location (36.7436 N, -121.88 E) shown with blue marker and arrow. Depths shown in meters. (reproduced from `https://www.nauticalcharts.noaa.gov/ENCOnline/enconline.html`)

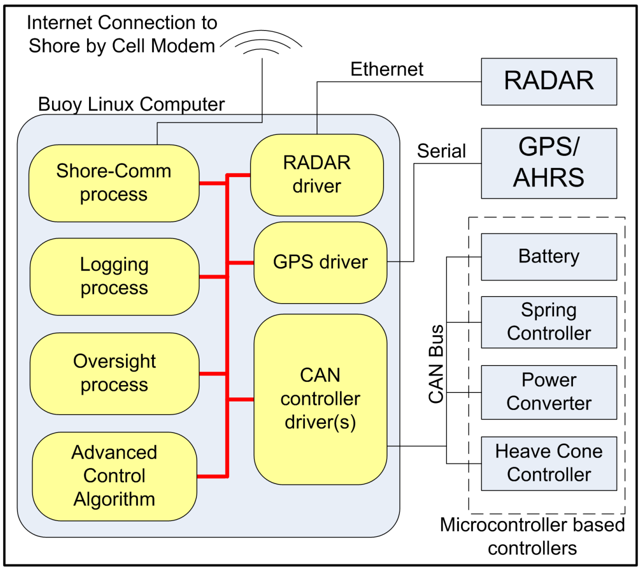

Fig. 3 MBARI-WEC buoy computing and software infrastructure.

micro-controllers has provided considerable software reliability in this system. The micro-controller processors do not rely on any third party operating systems, have no file system and are almost entirely stateless. In addition to interfacing with the micro-controllers, the Linux computer logs data from a GPS/IMU (Crossbow Nav440) and a SimRad radar system currently being used for incoming wave-detection research.

2.1 Buoy subassembly

A layout drawing of the MBARI-WEC buoy is shown in Fig. 4. On board the buoy are two watertight boxes: one contains the battery system and the other contains the buoy control Linux computer and associated hardware. The battery has a capacity of 5 kW-Hrs (17 A-Hrs @ 325 V) and this housing also includes a 325 V to 24 V power supply that is the main power supply to the buoy

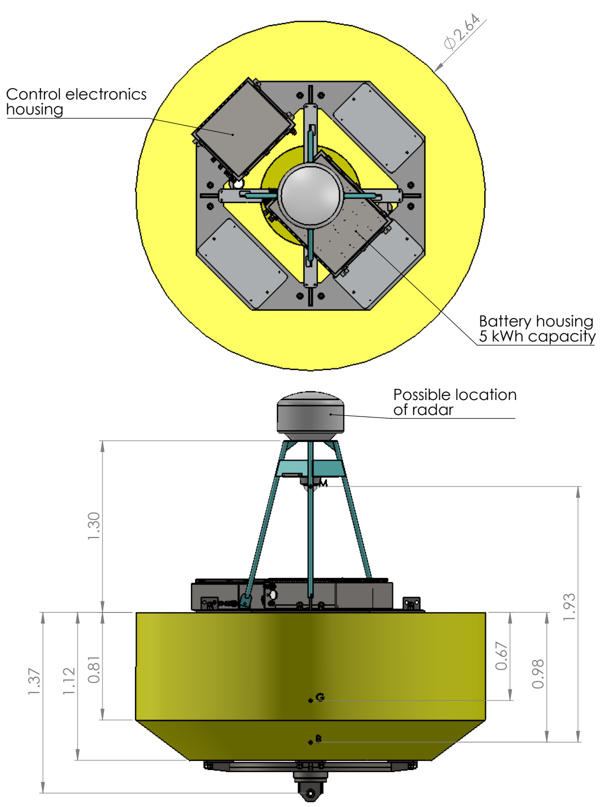

Fig. 4 MBARI-WEC buoy layout drawing with top and side views.

controller, a battery control micro-controller which provides power switching, manages over- and under-charge conditions as well as battery balancing, and monitors environmental conditions such as hydrogen levels and ground faults on the 325 V bus.

The controller box contains a Linux computer, an Ethernet network, a 2.4 Ghz Wi-Fi radio, a 4G cellular modem, power supplies that generate 12 V and 5 V from the incoming 24 V, and a power switching relay that can switch any voltage in this box to external devices as needed. Not shown in Fig. 4 are the antennas for the two radios (Wi-Fi and cellular modem), a light, and an independent satellite location transponder ("SPOT tracker").

2.2 Heave plate subassembly

The heave cone (Fig. 5) is located 30 m below the free surface, within the depth limit for a typical open water diver. The heave cone is designed to be adaptable and can open and close the center aperture by rotating the clover-shaped "trefoil" upon command for purposes of storm-survivability. The two configurations of the heave cone have dramatically different added mass values and modestly different drag coefficients. These values have been estimated by potential flow analysis and CFD studies, and have been confirmed in tank tests. The heave cone contains a micro-controller that controls the opening and closing of the doors, and also reports telemetry from a pressure sensor and inexpensive IMU (VectorNav VN-100). The Linux computer monitors PTO extension and opens the doors when larger seas cause excursions beyond 80% of the total stroke, and closes the doors upon a command from shore. This controller also contains a battery back-up and fail-safe logic that opens the doors in the case power or communications are lost from the surface. The tether from the PTO to the heave cone contains two larger power conductors and four smaller communications lines. Currently communication is provided by extending the system CAN bus down the tether and power is transmitted at 48 V.

2.3 PTO subassembly

The PTO system consists of an electro-hydraulic system for power capture and a pneumatic spring device that provides a restoring force (Fig. 6). These two elements (electro-hydraulic system and a pneumatic spring) are effectively connected in parallel. The PTO couples the buoy and heave cone via a flexible tether.

The pneumatic spring component provides a restoring force of about 8.9 kN (2000 lbs) per meter of extension. The static weight of the heave-cone therefore extends the PTO approximately half-way in calm seas. The pneumatic spring also contains a micro-controller that provides a variety of features. It is primarily a telemetry device that measures and reports (at 10-50 Hz) the spring extension, the upper and lower gas pressures, and the tension between the PTO and the surface buoy as measured by an 89 kN (20000 lb) load cell. Also present are a gas make-up pump that can (slowly) move gas from one side of the piston to the other, a gas re-

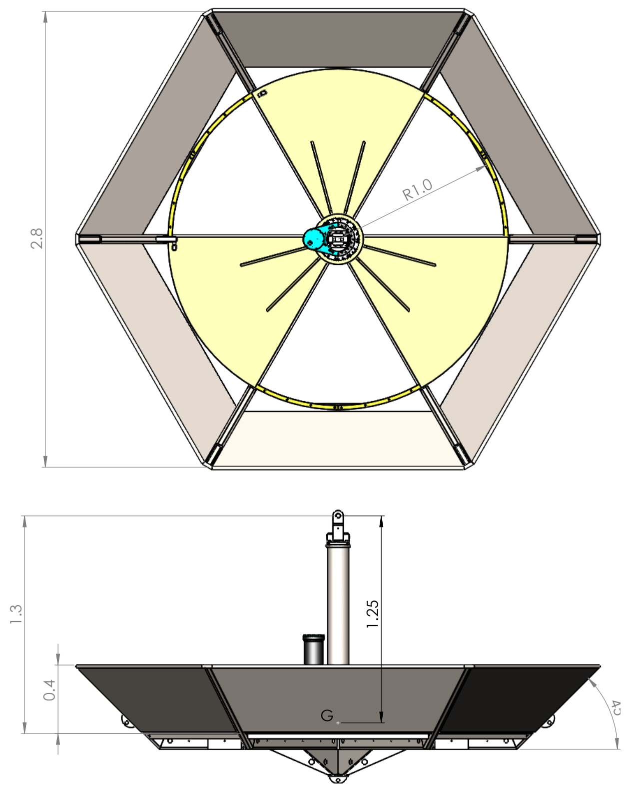

Fig. 5 MBARI-WEC heave cone layout drawing with top and side views.

lief valve that can reverse that process, and a switched power supply that provides 48 V to the heave-cone.

The electro-hydraulic device consists of a piston driving oil through a fixed displacement hydraulic motor that is directly coupled to a three-phase brushless motor/generator. There is no hydraulic rectification and the motor reverses rotary direction with a change in piston direction of motion. This component contains a 10 kW (peak) four-quadrant power converter that controls the current in the motor windings to a set value. If the prescribed torque opposes the motion of the motor, the system acts as a generator and boosts the voltage coming out of the three-phase generator to 325 V for transmission up to the battery pack on the buoy. This behaves as a current limited battery charger, if the batteries cannot accept the necessary power, the energy is directed instead to a submerged load-dump heater which is part of the PTO device. This load dump is sized to absorb all the power in case the batteries are full or disconnected.

If the commanded torque is in the same direction as the motion, the system acts as a motor and drives the ram with a force proportional to the commanded current. This draws energy out of the battery (up to a specified current limit). In addition to the current control duties, this micro-controller provides a range of telemetry to the buoy at 10-50 Hz, this data includes motor RPM, motor winding current which indicates torque, bus voltage, load dump current, battery current (plus or minus) as well as a variety of controller status bits.

By default, this controller acts in a standalone "linear generator" mode, in which the generator exerts a torque that is linearly proportional to the motor RPM. In the event that communications from the surface are lost, the system reverts to this linearly proportional control default. Alternatively, the buoy control computer can command any torque it likes based on an algorithm running top-side. In this case the power converter controller attempts to achieve the requested torque, but will self-limit in some situations for device safety considerations. Fig. 6 also shows the relation between the motor/drive, the load dump, and the battery system.

The motor-drive power electronics in this system were custom developed for this application because the wave-energy problem at this scale has some specific requirements that are hard to achieve using commercially available power electronics. In particular, the efficiency requirements of the system are important, especially at low speed. In this type of motor drive, switching losses in the transistors are a significant component of the total losses and unfortunately do not diminish at low speeds and winding currents like other resistive losses in the system. For this reason, the motor drive developed for the MBARI-WEC turns off the transistor bridge at low speeds/torques to eliminate this loss. Additional features that are atypical of commercially available systems are also required because of the autonomous and remote use of the system. Under-voltage, over-speed, and all other conditions must be handled gracefully and allow the system to continue operating. In particular, the system must also bootstrap itself and turn on in

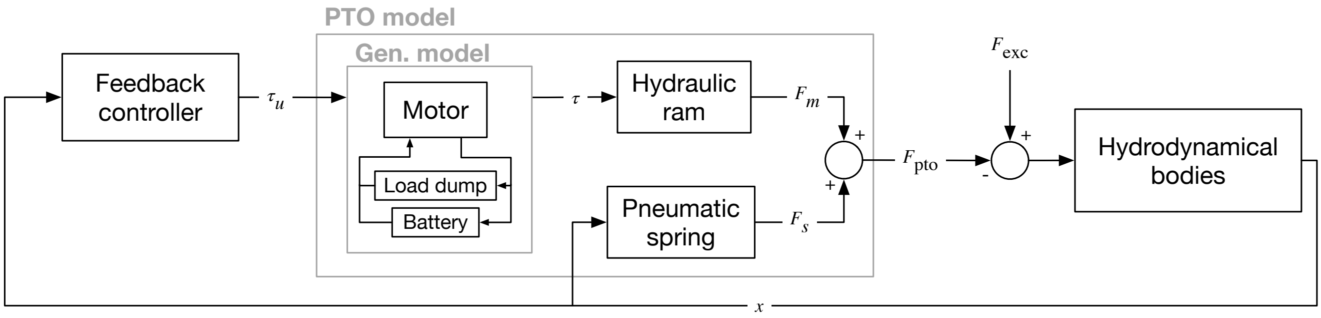

Fig. 6 PTO system electro-hydraulic block diagram.

the case of the batteries being disconnected, to ensure a load is always present in the system.

3 Hydrodynamic modeling

To enable future model-based system and control design, two hydrodynamic models have been developed: a frequency-domain model, which will provide a useful means of performing model based design (Section 3.1) and a time-domain model (Section 3.2) which provides a useful benchmark comparison point for the frequency-domain model.

3.1 Frequency-domain model

If we consider each of the two bodies within the device (the buoy and heave cone as described in Section 2) to be governed by an impedance model, we can write the equations of motion as follows.

$$\hat{Z}\,\hat{V} = \hat{F}_{\text{ext}} \tag{1}$$

Here, $\hat{Z} \in \mathbb{C}^{2\times 2\times n}$ is the complex impedance matrix, where n is the number of frequency components. The elements of the matrix are

$$\begin{aligned} \hat{Z}_{j,k}(\omega) &= B_{j,k}(\omega) + b_{j,k} \\ &\qquad + i\left(\omega\left(m_{j,k} + A_{j,k}\left(\omega\right)\right) - \frac{K_{j,k}}{\omega}\right) \\ &= R_{j,k}(\omega) + iX_{j,k}(\omega) \end{aligned} \tag{2}$$

The components $R_{j,k}(\omega)$ and $X_{j,k}(\omega)$ are the resistance and reactance, respectively. The terms $B_{j,k}(\omega)$ and $b_{j,k}$ are the frequency-dependent linear damping ("radiation damping") and additional linear damping (accounting for both viscous friction in the water and mechanical friction), respectively. Likewise, $A_{j,k}(\omega)$ and $m_{j,k}$ are the added and rigid-body inertias, respectively. Finally, $K_{j,k}$ is the balance of stiffness terms. In addition, the presence of the pneumatic spring in parallel with the hydraulic PTO coupling the two bodies (see Fig. 6), and the presence of a mooring affecting the heave plate, the stiffness term is

$$K = \begin{bmatrix} K_{hs,1} + K_{\text{spring}} & -K_{\text{spring}} \\ -K_{\text{spring}} & K_{hs,2} + K_{\text{spring}} + K_{moor} \end{bmatrix} \tag{3}$$

where K_{hs} is the hydrostatic stiffness. Similarly,

$$b_{2,2} = b_{drag,2} + b_{moor} \tag{4}$$

for the effect of the mooring line, b_{moor}. Values of $b_{drag,1}$ and $b_{drag,2}$ were based upon the iterative Lorentz linearization (Terra et al. 2005) of the quadratic drag coefficient in the heave direction for the buoy and heave plate using the periodic PTO forcing time series.

The complex velocity of each body described by $\hat{V} \in \mathbb{C}^{2\times n}$, where $\hat{V} = \left[\hat{V}_1,\, \hat{V}_2\right]^T$, where the buoy is body 1 and the heave cone is body 2. External forces on the system are given by $\hat{F}_{\text{ext}} \in \mathbb{C}^{2\times n}$. The external force is composed of two components: the excitation force, $\hat{F}_{\text{exc}}$, and the PTO force, $\hat{F}_{\text{pto}}$.

$$\hat{F}_{\text{ext}} = \hat{F}_{\text{exc}} - \hat{F}_{\text{pto}} \tag{5}$$

where the sign convention has the PTO force opposing the excitation (i.e., negative feedback) – this is also shown in Fig. 6. The PTO force acts in equal magnitude and opposite sign on bodies 1 and 2, such that

$$\hat{F}_{\text{pto}} = \begin{bmatrix} 1 \\ -1 \end{bmatrix} \hat{f}_{\text{pto}}, \tag{6}$$

where $\hat{f}_{\text{pto}} \in \mathbb{C}^{1\times n}$.

To find a simple means of specifying $\hat{f}_{\text{pto}}$, we can compress the system to a single degree of freedom by solving for the relative motion between the two bodies. First, returning to (1), we can write

$$\hat{V} = -\hat{Z}^{-1}\,\hat{F}_{\text{ext}}. \tag{7}$$

To solve for the relative motion, can further write

$$\begin{aligned} \Delta\hat{V} &= \hat{V}_1 - \hat{V}_2 = \begin{bmatrix} 1 & -1 \end{bmatrix} \hat{V} \\ &= -1 \begin{bmatrix} 1 & -1 \end{bmatrix} \hat{Z}^{-1}\,\hat{F}_{\text{ext}}. \end{aligned} \tag{8}$$

Within this composite system, in order to consider the impedance observed at the PTO we can disregard other external forces (i.e., by setting $\hat{F}_{\text{exc}} = 0$). Thus, from (8) we can find the composite system impedance.

$$\begin{aligned} \Delta\hat{V} &= -1 \begin{bmatrix} 1 & -1 \end{bmatrix} \hat{Z}^{-1}\hat{F}_{\text{pto}} \\ &= -1 \begin{bmatrix} 1 & -1 \end{bmatrix} \hat{Z}^{-1} \begin{bmatrix} 1 \\ -1 \end{bmatrix} \hat{f}_{\text{pto}} \\ &= \hat{Z}_{\text{eq}}^{-1}\hat{f}_{\text{pto}} \end{aligned} \tag{9}$$

The final expression of (9) gives defines the relative motion of the two bodies in the system in terms of a single PTO force, $\hat{f}_{\text{pto}}$, and an *equivalent* admittance, $\hat{Y}_{\text{eq}} = \hat{Z}_{\text{eq}}^{-1}$. Some manipulation of (9) gives

$$\hat{Y}_{\text{eq}} = \hat{Z}_{\text{eq}}^{-1} = \frac{\hat{Z}_{1,1} + \hat{Z}_{1,2} + \hat{Z}_{2,1} + \hat{Z}_{2,2}}{\hat{Z}_{1,2}\,\hat{Z}_{2,1} - \hat{Z}_{1,1}\,\hat{Z}_{2,2}}. \tag{10}$$

With (10), we now have a succinct means of describing the response of the WEC system to any input. Returning to the task of specifying $\hat{f}_{\text{pto}}$, we can maximize mechanical power by setting the PTO force based on the complex conjugate of the system impedance (see, e.g., Falnes 2002).

$$\begin{aligned} &\hat{f}_{\text{pto}} = \hat{Z}_{pto} \cdot \Delta\hat{V} \\ &\quad \text{where } \hat{Z}_{\text{pto, opt}} = \hat{Z}^{*}_{eq} \end{aligned} \tag{11}$$

As discussed in Bacelli and Coe (2020); Coe et al. (2020), the causal PTO impedance can be used to approximate the condition specified in (11) for some limited frequency range. Given the band-limited nature of ocean waves, the tuning of such a controller can be updated intermittently to track the slowly varying changes in sea state. This "self-tuning" approach was shown by Forbush et al. (2020). Thus, we can maximize power as follows.

$$\arg \min_{\hat{C}(k_p,k_i)} P(\hat{F}_{\text{exc}}, \hat{Z}_{eq}, \hat{C}(k_p, k_i)) \tag{12}$$

Here, the optimization problem has been defined to minimize work done by the WEC, such that negative work equates to absorbed power. The task defined by (12) is to minimize work done by the WEC by varying the controller gains k_p and k_i. Note that the solution to this problem is dependent on the prevailing sea state ($\hat{F}_{\text{exc}}$) and the device dynamics ($\hat{Z}_{eq}$).

3.2 WEC-Sim models

To provide a comparison point off which to judge the viability of using the impedance model described in Section 3.1, a weakly nonlinear time-domain model was developed in WEC-Sim (Ruehl et al. 2016). WEC-Sim

Table 2 Quadratic (C_d) drag coefficients and projected area (A) used in WEC-Sim in [heave, surge, pitch], and linear heave damping (B).

	C_d	A [m^2]	B [N-s/m]
Buoy	[1,1.15,0.5]	[5.47, 2.96, 5.47]	665.30
Cone	[* ,0.8, 1]	[6.56, 1.12, 6.56]	965.53

uses a time-domain Cummins' formulation (Cummins 1962) to model WEC dynamics and can be constructed from boundary element method (BEM) data, and expanded to model nonlinearity in the physical system. The specific sources of nonlinear behavior considered herein are kinematics, mooring, and a quadratic drag model based upon buoy and heave plate geometry (Table 2). In the case of the asymmetric heave cone, a direction-specific drag coefficient of 1.45 (moving upward) and 0.85 (moving downward) is used, the decoupling of the heave plate and buoy motion when the tether is slack, and the single-point catenary mooring.

Additionally, MoorDyn (Hall and Goupee 2015) can be used to model the mooring based solely upon physical component description and advise linear approximation (i.e., K_{moor}) in absence of test data. For this, a heave-only WEC-Sim model using MoorDyn model was run, and a least-squares fit linear pre-tension, spring, and damping approximation was developed relating mooring force to heave plate displacement and velocity.

$$\begin{bmatrix} K_{moor} \\ b_{moor} \\ T \end{bmatrix} = \begin{bmatrix} X_2 \; V_2 \; 1 \end{bmatrix} \backslash F_{\text{moorDyn}} \tag{13}$$

where X_2 and V_2 are the column vector time-series of heave displacement (m) and velocity (m/s) of the heave plate, F_{moorDyn} is the column vector time-series of mooring force as calculated by MoorDyn, and T is the mooring pre-tension (N). Because the suspended wet mass of the single-point catenary mooring will change based upon sea-level changes (i.e., tides) and the lateral and vertical displacement of the heave plate to the mooring anchor, this approximation is only anticipated to be valid in the vicinity of the linearized location (Table 3). However, excellent agreement was observed under these conditions ($r^2 = 0.99$).

Table 3 Linearized mooring parameters.

K_{moor} [N/m]	b_{moor} [N-s/m]	T [N]
6.47	81.14	233.22

Table 4 WEC-Sim model configurations for comparison with impedance model. Note that WS0 is not shown, but is the same as WS1, but with a rigid tether.

Model ID	DOF	Drag	Mooring
WS1	heave only	linear	matrix
WS2	planar motion	quadratic	matrix
WS3	planar motion	quadratic	MoorDyn

4 Comparison of hydrodynamical models

As the impedance model detailed in Section 3.1 will be used for control design, it is necessary to assess the accuracy of this model. Here, we compared the impedance model against a series of models developed in WEC-Sim. The different WEC-Sim model configurations are summarized in Table 4 and illustrated in Fig. 7. The WS1 model is a heave-only model with only linear dynamics. The WS2 model adds additional kinematics for planar motion (heave, surge, pitch) and quadratic drag. WS3 is a four-body model (float, PTO cylinder, tether, and heave cone), and is considered the closest approximation of the physical device used in this comparison.

By treating the WEC-Sim results as *numerical experiments*, system identification (SID) methods can be applied to produce linear impedance models (Bacelli et al. 2017; Pintelon and Schoukens 2012; Ljung 1999). In this case, the PTO was excited with a pink spectra from 0.015 to 1.5 Hz. Note that in WEC-Sim configuration WS1 - WS3, the slack tether decoupling was modeled, but PTO force amplitudes were selected such that the tether remained taut throughout all device motion. Fig. 8 shows a Bode plot with these admittance models, alongside the admittance model developed directly from the BEM coefficients per (10). The WEC-Sim results agree well with BEM estimates near the resonance peak of the heave cone single-body admittance, but the higher frequency resonance peak occurs at a slightly

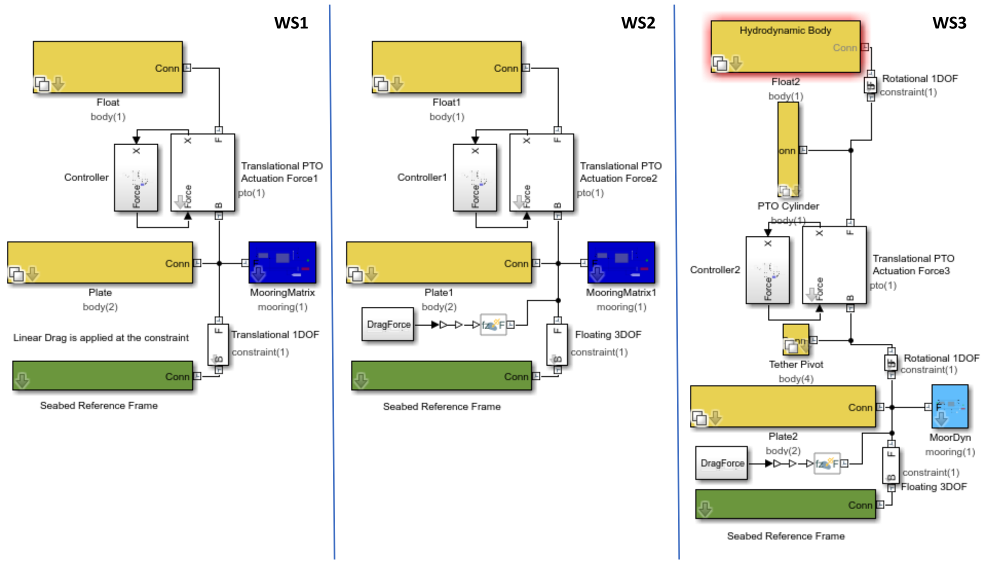

Fig. 7 Screenshots of WEC-Sim models in MATLAB Simulink showing different model configurations. See Table 4 for further explanation. Note that WS0 is not shown, but is the same as WS1, but with a rigid tether.

lower frequency than predicted from BEM, which itself agrees closely with the single-body buoy impedance.

While Fig. 8 conveys the matching of these models in linear terms, it is also necessary to understand how well the linear model captures the dynamics of the WEC (i.e., the amount of nonlinearity present in the system and not captured by a linear model). Fig. 9 shows the magnitude of velocity response from each of the four models in a regular wave with $H = 1.25\,\mathrm{m}$, $T = 8\,\mathrm{s}$, which is considered somewhat representative of the wave climate at the Monterey Bay deployment site during typical summer deployments.[1] An optimal linear damping of 851 Ns/m was applied via the PTO (Falnes 2002; Coe et al. 2020). Note that, per Fig. 8 and Table 1, this 8 s wave period is nearly the resonant frequency of the heave plate, and near the largest resonance peak of the equivalent impedance As a result, this case shows large-amplitude relative body motion, resulting in significant tether slack not captured in linear frequency-domain models (see time history in Fig. 10). For an additional point of comparison, a forth WEC-Sim configuration (WS0) was tested in which a rigid tether was modeled. Otherwise identical to WS1, WS0 performs equivalently when no tether slack occurs.

A contrasting sea-state, with $H = 1\,\mathrm{m}$, $T = 5.5\,\mathrm{s}$, not expected to cause tether slack was also simulated. In this case the optimal damping factor for the PTO is 943 Ns/m. The results of this case are shown in Fig. 11,

From Fig. 9 and Fig. 11, we can see the level of nonlinear content present in each model by the magnitude of the excited harmonics. The linear model, $\hat{Y_{eq}}$ contains effectively no energy at higher harmonics, but is presented here so the extent of numerical error can be evaluated. In the larger sea-state (Fig. 9), the substantial differences between WS0 and WS1 suggest that tether slack is the most significant source of nonlinearity; this can be confirmed by Fig. 10. Further, note that substantially less energy is contained at higher harmonics for WS1-WS3 in the smaller sea state (Fig. 11), again highlighting the significant effect of tether slack. In the smaller sea-state, where there is no tether slack, WS2 and WS3 demonstrate that the impact of quadratic drag and nonlinear mooring: energy at each higher harmonic increases monotonically from WS1 (identical to WS0) to WS3.

Quantitatively, we can also find the total harmonic distortion (THD) from each velocity signal (see Table 5). Again, the linear BEM solution has a theoretical

[1] Note that a regular wave is used here instead of an irregular wave to enable a more clear analysis of nonlinearities. However, in a real sea state the energy would be more broadly distributed across a range of frequencies.

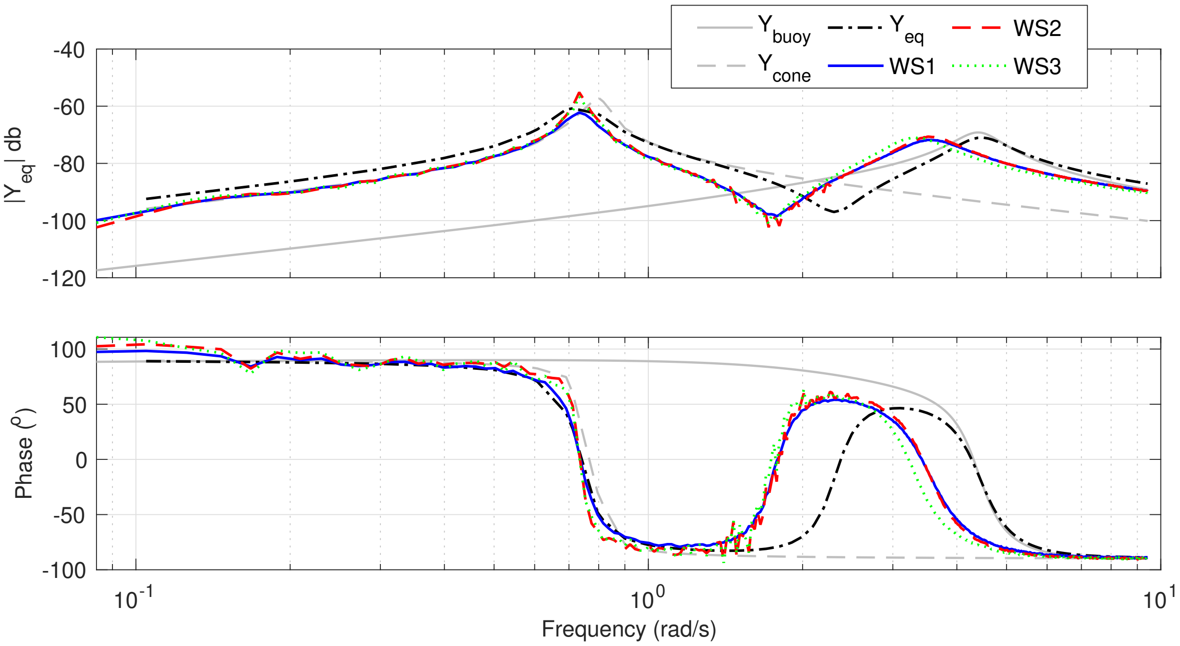

Fig. 8 Bode plot of admittance calculated from WEC-Sim models compared against system admittance directly from BEM coefficients. Single-body buoy and heave plate admittance are also shown.

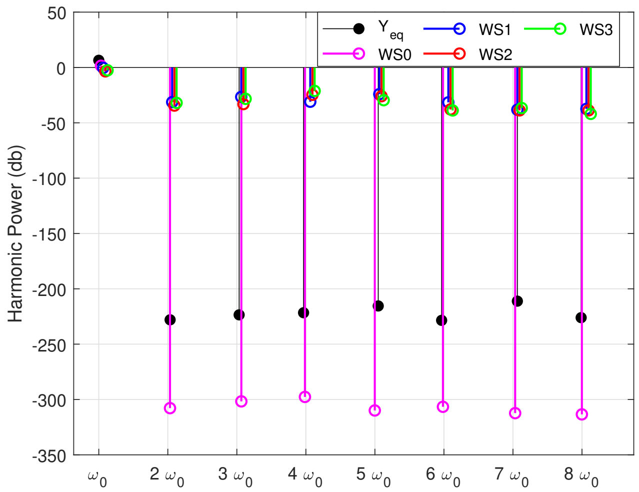

Fig. 9 Magnitude and phase response of models for a regular wave with $H = 1.25\,\mathrm{m}$, $T = 8\,\mathrm{s}$. All cases are evaluated at resonances of the excited frequency, minor offsets are introduced in the plot to avoid overlapping similar data.

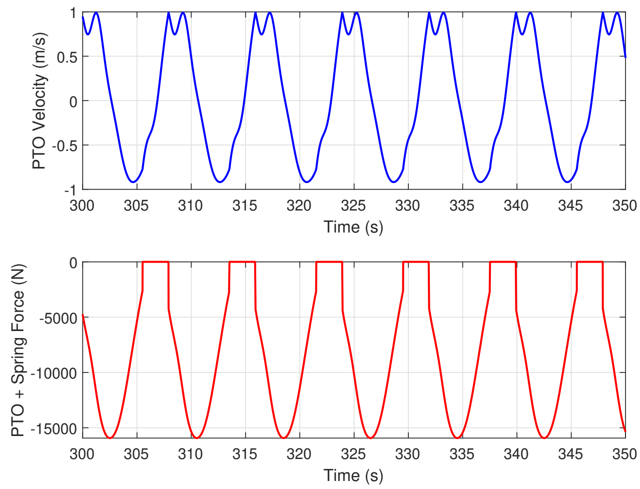

Fig. 10 PTO and spring force with PTO velocity for WS2 in $T = 8$, $H = 2.5$. The zeros of PTO and spring force indicate tether slack events.

Table 5 Percent total harmonic distortion for regular wave simulations.

Wave state	Y_{eq}	WS0	WS1	WS2	WS3
$T = 8\,\mathrm{s}$, $H = 1.25\,\mathrm{m}$	0.0	0.0	9.8	12.7	14.3
$T = 5.5\,\mathrm{s}$, $H = 1\,\mathrm{m}$	0.0	0.0	0.0	2.1	2.3

THD of zero, but is included here to quantify the extent of numerical error. Aligning with intuition, the progressive introduction of nonlinearities to simulation cases serves to increase the THD monotonically from WS0 to WS3, with the most striking separation occurring between WS0 and WS1, indicating that tether slack is the primary nonlinearity. Further, there is a striking reduction in THD for all cases in the smaller sea-state. However, it is notable that THD remains fairly low in all cases, suggesting that nonlinear will not strongly limit the utility of strictly linear models for controller development.

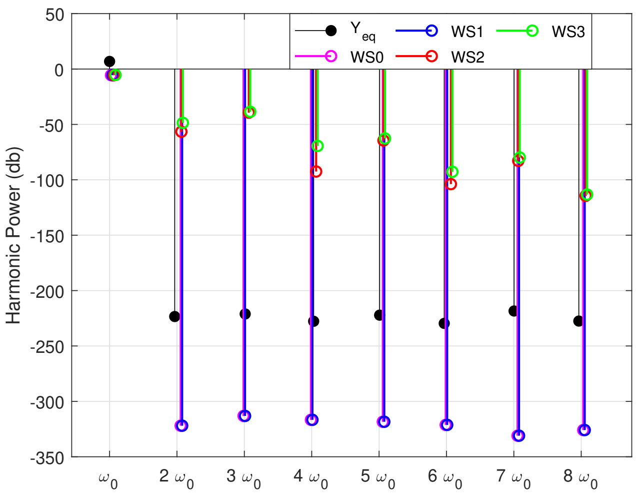

Fig. 11 Magnitude and phase response of models for a regular wave with $H = 1\,\mathrm{m}$, $T = 5.5\,\mathrm{s}$. All cases are evaluated at resonances of the excited frequency, minor offsets are introduced in the plot to avoid overlapping similar data.

5 Discussion

Generally, there is strong agreement in the identified systems observed for all WEC-Sim realizations (Fig. 8). Additionally, the nonlinearity in the WEC-Sim models are relatively small (see Fig. 11 and Table 5). This suggests that, at least for the excitation used here, nonlinearities have a minor impact, and in turn, that the linear impedance system model adequately describes complex system dynamics for the purposes of controller design. This is especially true if one considers that power is proportional to velocity squared.

It is interesting to note the disagreement between the admittance model and WS1, as shown Fig. 8. One potential source for this discrepancy is the infinite-frequency added mass ($A_\infty = \lim_{\omega\to\infty} A(\omega)$). WEC-Sim relies fundamentally on the time-domain Cummins' formulation, which uses an estimate of infinite-frequency added mass, along with impulse response functions, to determine WEC dynamics at each time-step via a convolution integral (see, e.g., Tom et al. 2015). Given the estimation methodology of commercial BEM codes, this implies that estimates of added mass coefficients must be available to a sufficiently high frequency and at a fine enough discretization such that they are resolved to their asymptotic limit.

Another factor to consider is varying levels of nonlinearity in the two regular wave test cases (see Table 5). This highlights the amplitude-dependency of system nonlinearity: the linear impedance model may be an adequate descriptor for small perturbations, but large sea-states may cause substantial deviation. However, in this particular case, tether slack is clearly undesirable from an operational perspective. Thus, a properly-designed controller may itself confine operations to a more-nearly linear regime. Avoiding significant nonlinear behavior may not be ideal or possible for all WEC and PTO archetypes, and the limitations of a linear model should be considered in the context of each specific device.

6 Conclusion

The MBARI-WEC is a first of its kind device with an extended deployment history. The device has been designed for support of autonomous sensors and to eventually support AUV charging. With roughly ten years worth of development and deployment experience, the MBARI-WEC has a plethora of learning experiences to offer.

This study has presented the particulars of the MBARI-WEC design for general reference. Additionally, frequency domain hydrodynamic model was derived and compared with similar models solved in the time domain via WEC-Sim. The comparison of these models shows that, in comparison to the higher fidelity WEC-Sim model, the frequency domain model does a good job of capturing the device dynamics. Nonlinearities seen in the WEC-Sim results tended to be small, especially when slack line events that would be avoided during actual operation did not occur. These findings support the application of the frequency domain model for future co-design efforts to improve the performance of the MBARI-WEC.

Future efforts will include an in-depth analysis of the MBARI-WEC PTO, with experimental and numerical modeling. Additionally, measurements from wave buoys and hindcast data will be used in combination with device telemetry to further validate the hydrodynamic models proposed in this paper. These analyses will support design improvements to the system. One potential point of interest will be the investigation of ways in which the WEC system and control design can be modified to improve performance, specifically to reduce loading in large sea states and improve power generation in smaller sea states. MBARI's experience with this system to date indicates that an important improvement to pursue is to make the system smaller, as a 10-20% reduction in size would simplify deployment and use significantly. Currently, no advanced control systems have been implemented for this system, so this is an important area of research that can help meet the size goals of the system without sacrificing the energy captured.

Acknowledgements Sandia National Laboratories is a multi-mission laboratory managed and operated by National Technology and Engineering Solutions of Sandia, LLC., a wholly owned subsidiary of Honeywell International, Inc., for the U.S. Department of Energy's National Nuclear Security Administration under contract DE-NA0003525. This paper describes objective technical results and analysis. Any subjective views or opinions that might be expressed in the paper do not necessarily represent the views of the U.S. Department of Energy or the United States Government.

Conflict of interest

The authors declare that they have no conflict of interest.

References

Bacelli G, Coe RG (2020) Comments on control of wave energy converters. IEEE Transaction on Control System Technologies pp 1–4, DOI 10.1109/TCST.2020.2965916, URL https://ieeexplore.ieee.org/document/9005201

Bacelli G, Coe RG, Patterson D, Wilson D (2017) System identification of a heaving point absorber: Design of experiment and device modeling. Energies 10(10):472, DOI 10.3390/en10040472, URL http://www.mdpi.com/1996-1073/10/4/472

Coe RG, Bacelli G, Forbush D (2020) A practical approach to wave energy modeling and control. Renewable and Sustainable Energy Reviews (submitted) DOI 10.36227/techrxiv.12939488.v1, URL https://www.techrxiv.org/articles/preprint/A_practical_approach_to_wave_energy_modeling_and_control/12939488

Cummins WE (1962) The impulse response function and ship motions. Tech. Rep. DTNSDRC 1661, Department of the Navy, David Taylor Model Basin, Bethesda, MD, URL http://dome.mit.edu/handle/1721.3/49049

Driscol BP, Gish LA, Coe RG (2020) A scoping study to determine the location-specific wec threshold size for wave-powered auv recharging. IEEE Journal of Oceanic Engineering pp 1–10, DOI 10.1109/JOE.2020.2973032, URL https://ieeexplore.ieee.org/document/9044418

Falnes J (2002) Ocean Waves and Oscillating Systems. Cambridge University Press, Cambridge; New York

Falnes J, Hals J (2012) Heaving buoys, point absorbers and arrays. Philosophical Transactions of the Royal Society A: Mathematical,Physical and Engineering Sciences 370(1959):246–277, DOI 10.1098/rsta.2011.0249, URL http://rsta.royalsocietypublishing.org/content/370/1959/246.abstract, http://rsta.royalsocietypublishing.org/content/370/1959/246.full.pdf+html

Forbush DD, Bacelli G, Spencer SJ, Coe RG (2020) A self-tuning WEC controller for changing sea states (in press). In: Proceedings of the 21st IFAC World Congress

Green R, Copping A, Cavagnaro RJ, Rose D, Overhus D, Jenne D (2019) Enabling power at sea: Opportunities for expanded ocean observations through marine renewable energy integration. In: OCEANS 2019 MTS/IEEE SEATTLE, IEEE, Seattle, WA, USA, pp 1–7, DOI 10.23919/OCEANS40490.2019.8962706, URL https://ieeexplore.ieee.org/document/8962706

Hagerman G (2002) Wave energy systems for recharging auv energy supplies. In: Proceedings of the 2002 Workshop on Autonomous Underwater Vehicles, 2002., IEEE, San Antonio, TX, USA, pp 75–84, DOI 10.1109/AUV.2002.1177207, URL https://ieeexplore.ieee.org/document/1177207

Hall M, Goupee A (2015) Validation of a lumped-mass mooring line model with DeepCwind semisubmersible model test data. Ocean Engineering 104:590–603, DOI 10.1016/j.oceaneng.2015.05.035, URL https://www.sciencedirect.com/science/article/pii/S0029801815002279

LiVecchi A, Copping A, Jenne D, Gorton A, Preus R, Gill G, Robichaud R, Green R, Geerlofs S, Gore S, et al. (2019) Powering the blue economy; exploring opportunities for marine renewable energy in maritime markets. Tech. rep., US Department of Energy, Office of Energy Efficiency and Renewable Energy. Washington, DC, Washington, DC, URL https://www.energy.gov/sites/prod/files/

2019/03/f61/73355.pdf
Ljung L (1999) System identification - Theory for the User. Prentice-Hall
Pintelon R, Schoukens J (2012) System identification: A frequency domain approach. John Wiley & Sons
Ruehl K, Michelen C, Bosma B, Yu YH (2016) WEC-Sim phase 1 validation testing: Numerical modeling of experiments. In: Proceedings of the ASME 2016 35th International Conference on Ocean, Offshore and Arctic Engineering (OMAE), American Society of Mechanical Engineers, ASME, Busan, South Korea, pp V006T09A026–V006T09A026, DOI 10.1115/OMAE2016-54986, URL https://doi.org/10.1115/OMAE2016-54986
Terra GM, van de Berg WJ, Maas LR (2005) Experimental verification of Lorentz' linearization procedure for quadratic friction. Fluid Dynamics Research 36(3):175, DOI 10.1016/j.fluiddyn.2005.01.005, URL https://iopscience.iop.org/article/10.1016/j.fluiddyn.2005.01.005
Tom N, Lawson M, Yu YH (2015) Demonstration of the recent additions in modeling capabilities for the WEC-Sim wave energy converter design tool. In: Proceedings of the ASME 2015 34th International Conference on Ocean, Offshore and Arctic Engineering (OMAE), American Society of Mechanical Engineers, ASME, St. John's, Newfoundland, Canada, vol 56574, p V009T09A035, DOI 10.1115/OMAE2015-42265, URL https://doi.org/10.1115/OMAE2015-42265

A System telemetry

Table 6 provides a listing of system telemetry as of the publication of this paper.

Table 6 MBARI-WEC system telemetry.

Signal name	Description
Battery Controller (BC)	
BC_Time	Unix time of each data point
BC_Voltage	Main battery voltage
BC_GroundFault	0-20mA output from Bender ground fault detector
BC_Ips	Current flowing to the 300 V-24 V power supply for Linux buoy controller and accessories.
BC_VStopCharge	Voltage indicating number of 12 V batteries that are at or above the specified “StopCharge” voltage
BC_Hydrogen	% of LEL of H2 in battery box
BC_Status	A variety of status bits indicating the state of the battery system
BC_VBalance	A status voltage that indicates how many cells are currently bypassing in balancing mode.
BC_VStopCharge	A status voltage that indicates how many cells are over-voltage, this tells the power converter to back off the voltage
BC_Voltage	Battery pack voltage
BC_GroundFault	4-20 mA signal from Bender ground fault detector indicating ground faults on 300 V bus
Power Converter (PC)	
PC_Time	Unix time of each data point
PC_BattCurr	Current flowing to or from batteries
PC_Voltage	Bus voltage at power converter
PC_RPM	Motor shaft speed (positive RPM corresponds to PTO ram retracting)
PC_WindingCurrent	Winding Quadrature Current, linearly related to torque
PC_LoadCurr	Current flowing to the load dump
PC_Status	A variety of status bits indicating state of the power conveter
PC_DiffPress	0-10 psi (0-0.69 bar) signal indicating hydraulic compensator pressure above ambient
PC_Scale	User specified scale factor (0.5:1.2) applied to internally programmed torque/speed curve
PC_Retract	User specified factor (0.5:1.2) applied to internally programmed torque/speed curve during retraction only
Spring Controller (SC)	
SC_Time	Unix time of each data point
SC_LoadCell	0-20000 lb (0-89 kN) load cell reading, between PTO and buoy
SC_LowerPressure	Lower spring chamber pressure (psia)
SC_UpperPressure	Upper spring chamber pressure (psia)
SC_Range	PTO Ram position in inches (0: fully retracted; 80: fully extended).
SC_Status	A variety of status bits indicating state of the spring controller
Heave Cone Controller (TC)	
TC_Time	Unix time of each data point
TC_Accel1	Heave Cone x-accelertion (m/s^2)
TC_Accel1	Heave Cone y-accelertion (m/s^2)
TC_Accel1	Heave Cone z-accelertion (m/s^2)
TC_Qtn1	Heave Cone Orientation Quaternion
TC_Qtn2	Heave Cone Orientation Quaternion
TC_Qtn3	Heave Cone Orientation Quaternion
TC_Qtn4	Heave Cone Orientation Quaternion
TC_Mag1	Heave Cone Magnatometer Component 1
TC_Mag2	Heave Cone Magnatometer Component 2
TC_Mag3	Heave Cone Magnatometer Component 3
SC_Status	Heave Cone Trefoil Position and Status
Buoy GPS/IMU (XB)	
XB_Time	Unix time of each data point
XB_Alt	Buoy Vertical Position
XB_Lat	Latitude from GPS
XB_Lon	Longitude from GPS
XB_NorthVel	North Buoy Velocity (m/s)
XB_EastVel	East Buoy Velocity (m/s)
XB_DownVel	Vertical Buoy Velocity (m/s)
XB_YawAng	Buoy Yaw Angle (rad).
XB_PitchAng	Buoy Pitch Angle (rad).
XB_RollAng	Buoy Roll Angle (rad).